

Available online at [www.sciencedirect.com](http://www.sciencedirect.com)

**jmr&t**  
Journal of Materials Research and Technology  
journal homepage: [www.elsevier.com/locate/jmrt](http://www.elsevier.com/locate/jmrt)



## Original Article

# The effect of surface treatment and orientation on fatigue crack growth rate and residual stress distribution of wire arc additively manufactured low carbon steel components



Anna Ermakova <sup>a</sup>, Javad Razavi <sup>b</sup>, Sandra Cabeza <sup>c</sup>, Elzbieta Gadalinska <sup>d</sup>, Mark Reid <sup>e</sup>, Anna Paradowska <sup>e,f</sup>, Supriyo Ganguly <sup>g</sup>, Filippo Berto <sup>b</sup>, Ali Mehmanparast <sup>a,\*</sup>

<sup>a</sup> Department of Naval Architecture, Ocean and Marine Engineering, University of Strathclyde, Glasgow G1 1XQ, United Kingdom

<sup>b</sup> Norwegian University of Science and Technology (NTNU), Trondheim, Norway

<sup>c</sup> Institut Laue-Langevin (ILL), Grenoble, France

<sup>d</sup> Lukasiewicz Research Network – Institute of Aviation, Warsaw, Poland

<sup>e</sup> Australian Centre for Neutron Scattering, Sydney, Australia

<sup>f</sup> School of Civil Engineering, The University of Sydney, Sydney, Australia

<sup>g</sup> Welding Engineering and Laser Processing Centre, Cranfield University, Cranfield MK43 0AL, United Kingdom

## ARTICLE INFO

## Article history:

Received 7 February 2023

Accepted 31 March 2023

Available online 5 April 2023

## Keywords:

Directed energy deposition

Wire arc additive manufacturing

Fatigue

Surface treatment

Residual stress

## ABSTRACT

The directed energy deposition (DED) processes, such as laser metal deposition or Wire Arc Additive Manufacturing (WAAM), are gradually becoming the preferred method for fabrication of large-scale components using metal additive manufacturing (AM) technology. In this work, the possibility of fatigue life enhancement in WAAM built low carbon steel components, by means of rolling and laser shock peening surface treatment techniques, was investigated. A series of fatigue crack propagation tests were performed on surface treated ER70S-6 and ER100S-1 WAAM built specimens, and the results were analysed and compared with the untreated materials tested under the same loading conditions. The obtained results were interpreted in terms of the sensitivity of the cracking behaviour to the specimen orientation and extraction location. Furthermore, the residual stress profiles were measured, before and after applying the surface treatment techniques, and the effects of locked-in residual stresses on the fatigue performance of WAAM built components were discussed. Finally, a detailed texture analysis was performed on the surface treated and untreated regions of both WAAM built materials considered in this work. The obtained results from this study provide an insight into the advantages and disadvantages of various surface treatment techniques for fatigue life enhancement of WAAM built components with the view to extend the application of this advanced manufacturing technology to a wider range of industrial applications.

© 2023 The Author(s). Published by Elsevier B.V. This is an open access article under the CC BY license (<http://creativecommons.org/licenses/by/4.0/>).

\* Corresponding author.

E-mail address: [ali.mehmanparast@strath.ac.uk](mailto:ali.mehmanparast@strath.ac.uk) (A. Mehmanparast).

<https://doi.org/10.1016/j.jmrt.2023.03.227>

2238-7854/© 2023 The Author(s). Published by Elsevier B.V. This is an open access article under the CC BY license (<http://creativecommons.org/licenses/by/4.0/>).

**Nomenclature**

$a_0$	initial crack length in C(T) specimen
$a_i$	instantaneous crack length
$a_{i,p}$	initial crack length in C(T) specimen after pre-fatigue cracking
$a_{f,c}$	estimated final crack length at the end of the test
$\Delta a$	crack extension
B	total thickness of C(T) specimen
$C_i$	instantaneous unloading compliance
$d_0$	Stress-free reference point for lattice spacing
$d$	lattice spacing
E	Young's modulus
H	height of C(T) specimen
$hkl$	Miller indices
J	the power density in laser shock peening process
K	stress intensity factor
N	number of cycles
n	Paris-law constant
$P_{max}$	maximum load in a fatigue cycle
$P_{min}$	minimum load in a fatigue cycle
R	load ratio
W	width of C(T) specimen
$\epsilon$	residual strain
$\eta$	geometry dependent function
$\theta$	scattering angle
$\lambda$	neutron wavelength
$\nu$	Poisson's ratio
$\sigma_i$	stress component
$\sigma_Y$	yield stress
AM	Additive Manufacturing
AV	Average data
B	Bottom
C(T)	Compact Tension specimen geometry
CMT	Cold Metal Transfer
DED	Directed Energy Deposition
EBSD	Electron Backscatter Diffraction
EDM	Electrical Discharge Machining
FEA	Finite Element Analysis
FCG	Fatigue crack growth
H	Horizontal
IPF	Inverse pole figures
LP	Laser peening surface treatment
MN	Mean line
MUD	Multiple of uniform density
ND	Neutron diffraction
R	Rolling surface treatment
SD	Standard deviation
SIF	Stress intensity factor
T	Top
V	Vertical
WAAM	Wire Arc Additive Manufacturing
XR	X-ray

**1. Introduction**

Fatigue is known as one of the main modes of failure in engineering structures, which are often subjected to cyclic loading conditions. Mechanical and fracture properties of alloys employed in engineering structures can be dramatically influenced by operation under severe environmental conditions such as harsh corrosive environments, leading to premature failure of structures and components during their service life [1]. Therefore, there is an essential need to improve the fatigue performance of engineering structures in order to achieve prolonged lifespans. Historically, a number of mechanical and surface treatment techniques have been developed and implemented for fatigue life enhancement purposes in industrial applications. An example of the mechanical technique, which is widely utilised to obtain extended fatigue lives in various industrial applications, is grinding. Using this technique, the stress concentration zones, particularly at the weld toes, are eliminated to reduce the local stress levels hence increasing the fatigue life [2]. In addition to the mechanical techniques, various surface treatment methods are available to use in isolation or in conjunction with mechanical design modifications. The most well-known surface treatment techniques which are implemented in a wide range of industrial applications are shot peening [3–7], laser shock peening [8–10], deep cold rolling [11–15], and vibro peening [16]. The general idea behind the surface treatment approach is to introduce a protective layer of compressive residual stresses that will decelerate crack initiation and propagation at the outer surface of the engineering components or structures. However, the extent of complexity, cost, required penetration depth and efficiency of different surface treatment techniques heavily depend on the material properties and operational loading conditions. Moreover, the formation of strain hardening and residual stresses during the surface treatment processes will alter the metallurgical features, hence the effects of microstructural changes on subsequent fatigue behaviour need to be fully investigated and understood for a given material and loading condition [1].

An efficient directed energy deposition (DED) process for metal additive manufacturing (AM) which has been found suitable for fabrication of large-scale components and structures is the wire arc additive manufacturing (WAAM) technology. This DED manufacturing technique, which can also be implemented for re-manufacturing and repair purposes, produces near shape components without the need for complex tooling or moulds. WAAM offers an immense potential for significant savings in cost, lead time and material waste as well as increased material efficiency and improved component performance [17,18]. However, the welding-based manufacturing process introduces residual stresses and distortions that would impact the fatigue life and may facilitate the crack initiation and propagation process in the WAAM built parts [19–21]. Also, another disadvantage of the WAAM process is the pronounced surface waviness that may introduce higher stress concentration sites between additively

welded layers, which would undermine the fatigue performance [22]. For successful implementation of the WAAM method, the material properties should ideally meet or exceed those for the wrought counterparts. This can be difficult to achieve due to a considerably different manufacturing process that WAAM parts undergo, which involves a series of thermal cycles and continuous re-heating and cooling which will greatly affect the microstructure of the WAAM part [23]. In order to address the challenges that the WAAM technology brings, the surface treatment techniques were implemented in several studies with a view to improve the structural response and material characteristics of the additively manufactured parts.

The most common surface treatment method for life enhancement of WAAM parts that has been investigated in previous studies is inter-pass rolling that is normally applied on top of each deposited layer while building the WAAM parts. Colegrove et al. [24] concluded that inter-pass rolling of the deposited layers improved the mechanical properties of Ti–6Al–4V WAAM parts through microstructural refinement, increasing both the yield and tensile strength by up to 25%. Also, this method improved the fatigue properties due to high proof strength. The reported improvement may be also due to the reduced amount of induced porosity, which is known to degrade the fatigue performance. A different study [25] concluded that the effect of inter-pass rolling is reduced if rolling is applied on every fourth deposited layer, instead of each individual layer. In the research by Hönnige et al. [26], the rolling process was implemented on aluminium WAAM walls, and the results confirmed the efficiency of the treatment method to harden the material and improve the yield and tensile strength. Significant reduction of the peak residual stresses in longitudinal direction (i.e. WAAM building direction) was observed in several research studies by using inter-pass rolling on thin stainless steel and titanium WAAM walls [27,28]. The results have shown that the locked-in tensile residual stresses changed to compressive stresses after the surface treatment was applied. Similar effect of surface rolling on residual stress state was reported on wrought steel parts [29]. Moreover, it was concluded that the induced residual stress value using the rolling technique can be controlled by the magnitude of the applied pressure during rolling process.

Laser shock peening, which is often referred to as laser peening (LP), generally improves the resistance of metals and alloys to fatigue failure, by introducing strain hardening and compressive residual stresses into the part's surface using high energy pulsed laser source. The compressive residual stresses introduced by laser peening penetrate deeper below the surface than those from rolling or shot peening, usually resulting in higher fatigue life enhancement [3,8]. Thus, laser peening is commonly used for the mechanical components that have notches, holes or corners prone to fatigue failure, and potentially can help to overcome the limitations of the

WAAM technology [30]. In the study by Sun et al. [31], application of LP post-processing method on aluminium WAAM specimens exhibited a significant refinement of the microstructure, improvements of micro-hardness, transition of damaging tensile residual stresses to beneficial compressive stresses, and an increase in yield strength by 72%. Comparable results were reported by Chi [32] and Luo [33], on tested titanium WAAM specimens, confirming the effectiveness of the surface treatment method for enhancement of mechanical characteristics of the material. Significant grain refinement was observed in microstructure of WAAM specimens treated with LP [34]. While various researchers conducted a limited number of aerospace application related studies to investigate the role of LP effects on the mechanical response of the aluminium and titanium WAAM parts, currently there is no published data available in the open literature on LP surface treatment effects on fatigue performance of WAAM steel parts.

The main focus of the present study is to thoroughly investigate the influence of two surface treatment techniques, rolling and laser shock peening, on fatigue crack propagation behaviour of WAAM built specimens made with two different grades of steel ER70S-6 and ER100S-1. The fatigue performance of surface treated specimens is assessed and discussed by considering the specimen extraction orientation and location with respect to the WAAM built geometry. Moreover, the residual stress state is measured and compared before and after applying the surface treatment to evaluate the efficiency of the treatment methods on the fatigue performance of the WAAM parts. Last but not least, the material microstructure and texture were carefully examined and presented in this work. The strategic target of this study is to unlock the great potential of the WAAM technique for manufacturing, re-manufacturing and repair of offshore renewable energy structures. This would offer significant cost savings, particularly during the operation and maintenance phase of the asset life management and unveils the outstanding advantages of the WAAM technology to produce and maintain smart steel structures.

## 2. Materials and fabrication method

In the current study two types of steel welding wires were selected and employed, which are ER70S-6 [35] and ER100S-1 [36]. The chemical composition of these two steel wires is summarised in Table 1. Using each of these steel wires, a single WAAM wall was manufactured by the cold metal transfer (CMT) process, with the parameters shown in Table 2. Therefore, two thick WAAM walls were fabricated in total, with thickness of approximately 24 mm. The manufacturing set up, which is shown in Fig. 1, consisted of a CMT power source and a programmed robotic arm with a CMT torch,

**Table 1 – Chemical composition of the WAAM wires (wt.-%) [35,36].**

	C	Mn	Cr	Si	Ni	Mo	S	P	Cu	V
ER70S-6	0.09	<1.60	0.05	0.09	0.05	0.05	0.007	0.007	0.20	0.05
ER100S-1	0.08	1.70	0.20	0.60	1.50	0.50	–	–	–	–

**Table 2 – CMT-WAAM fabrication parameters.**

Shielding gas	Ar+20% CO <sub>2</sub>
Gas flow rate	15 L/min
Robot travelling speed	7.33 mm/s
Wire diameter	1.2 mm
Wire feed speed	7.5 m/min
Dwell time	120 s

which supplied both the welding wire and shielding gas during the fabrication process. Using an oscillation method [37], which is suitable for building thick WAAM walls, each wall was deposited on a base plate which was made of EN10025 rolled structural steel. As seen in Fig. 1, the base plate was attached onto the working table with eight clamps, to minimise bending and distortion of the plate due to high manufacturing temperatures. The clamps were removed upon completion of the deposition process, after the WAAM walls were cooled down to ambient temperature. The mechanical and fracture properties of WAAM built specimens made with both materials were investigated and presented in a previous study by Ermakova et al. [38].

Four notched compact-tension, C(T), specimens were then extracted from each of the WAAM walls using the Electrical Discharge Machining (EDM) method. Out of four C(T) specimens extracted from each material, two were machined from the top (T) of the wall while the other two were from the bottom (B). Also, for each of the extraction locations, the samples were extracted in two different orientations: vertical (V) – with the crack growth direction through AM layers, and horizontal (H) – with the crack path along AM layers. The combination of different specimen locations and orientations is schematically presented in Fig. 1. The C(T) specimens were designed according to the ASTM E647 standard [39] with the width of  $W = 50$  mm, height of  $H = 60$  mm, total thickness of  $B = 16$  mm and the initial crack length  $a_0 = 17$  mm (before pre-fatigue cracking). Knife edges were machined at the crack mouth of the specimens following the instructions in the ASTM 1820 standard [40], to accommodate a clip gauge for crack growth monitoring using the compliance measurement technique during the fatigue crack growth tests.

### 3. Application of surface treatment on WAAM built specimens

Upon extraction of eight C(T) specimens from the WAAM walls, four made of ER70S-6 and four made of ER100S-1, surface treatment techniques were applied onto the test specimens. For each of the two materials considered in this study, half of the specimens were treated with the rolling technique and another half with laser shock peening method, to assess the fatigue life enhancement performance of these two surface treatment techniques compared to untreated material state.

#### 3.1. Surface rolling

Two C(T) specimens extracted from the top of the ER70S-6 WAAM wall, denoted 70-VT and 70-HT, and two specimens

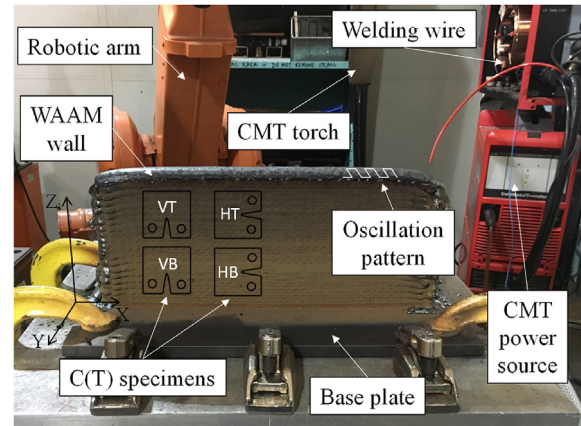


**Fig. 1 – WAAM-CMT system set up with schematic specimen extraction map.**

cut from the ER100S-1 WAAM wall, denoted 100-HT and 100-HB (see Fig. 1), were selected for surface rolling (R) treatment. The rolling parameters were adopted from the finite element analysis (FEA) study of Pi et al. [41], where it was suggested to use a 20 mm wide roller with a diameter of 50 mm made of a high-strength steel and apply rolling starting from the crack tip of the C(T) specimens with 80 kN load, moving along the crack path with a radial speed of 100 mm/s. The results from this FEA study [41] also showed that the optimum residual stress distribution was achieved by rolling the specimen for only 8 mm from the crack tip. Hence, the proposed parameters were implemented for the high pressure rolling on the C(T) specimens in the current study. The surface rolling treatment set up is shown in Fig. 2 (a). As seen in this figure, the rolling process consisted of a moving frame with a roller, laser tag for specimen alignment and three clamps to prevent the C(T) specimens from any movements. Each specimen was rolled on both sides (i.e., free surfaces). This was done by performing the surface rolling on the first side and then the specimen was flipped around to repeat the surface rolling treatment on the opposite side. A rectangular rolled surface area with the dimensions of  $20 \times 8$  mm was introduced ahead of the crack tip in C(T) specimens, which is visible in Fig. 2 (b).

#### 3.2. Laser shock peening

The remaining four C(T) specimens, two extracted from the ER70S-6 WAAM wall denoted 70-VB and 70-HB, and two cut from the ER100S-1 WAAM wall denoted 100-VT and 100-VB, were used to apply laser shock peening surface treatment technique. The treated area was identical to the rolled area (see Fig. 2 (b)) for direct comparison between the two surface treatment techniques. Similar to the surface rolling treatment, the LP treatment was applied on both sides of the C(T) specimens with a  $20 \times 8$  mm<sup>2</sup> rectangular treated area ahead of the notch tip. The laser shock peening treatment was applied onto the C(T) specimens using the spot size of 3 mm<sup>2</sup>, energy level of 8.1 with the power density of  $J = 5$  GW/cm<sup>2</sup>, pulse duration of 18 ns, with three layers providing 300% coverage. An example of the specimen during the laser shock



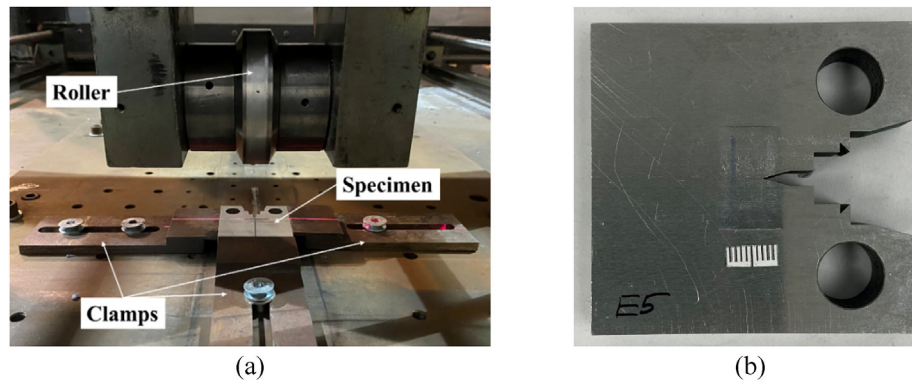


Fig. 2 – Surface rolling process: (a) treatment set up, and (b) an example of a rolled surface on a C(T) specimen.

peening process with a patch attached onto the specimen is displayed in Fig. 3 (a). An example of a specimen after LP treatment is shown in Fig. 3 (b), where the treated area is visible on the specimen surface.

#### 4. Residual stress measurements on WAAM built specimens

Two non-destructive residual stress measurement techniques were used to characterise the residual stress distribution profiles in the C(T) specimens extracted from the WAAM walls: neutron diffraction and X-ray methods. The neutron diffraction (ND) technique was used to measure the change in residual stresses in WAAM built specimens before and after the surface treatment application. This method offers a much deeper penetration depth for residual stress measurements compared to other non-destructive methods, allowing the characterisation of the three components of stress, hence was found suitable for residual stress characterisation in 16 mm thick C(T) specimens examined in this study. Subsequently, the X-ray (XR) method was used to measure the residual stresses after the introduction of the surface treatment. This method offers high resolution and accuracy over a thin layer on the outer surface of metallic components, hence was found suitable to measure near surface residual stresses which were

introduced into the WAAM built C(T) specimens by applying the surface treatment techniques. The details of the neutron diffraction and X-ray residual stress measurement techniques are described below. Two representative specimens extracted from the ER100S-1 WAAM wall were measured in this study to investigate the impact of surface treatment on residual stress distribution in WAAM built components at the neutron diffraction facilities.

##### 4.1. Neutron diffraction technique

In the current study, the initial residual stresses in four untreated ER100S-1 WAAM specimens were measured by a monochromatic strain diffractometer SALSA at the Institut Laue-Langevin (ILL)-France [42]. Upon completion of the surface treatment on these four specimens, the changes in the residual stress state were examined using the KOWARI strain scanner at the Australia's Nuclear Science and Technology Organisation (ANSTO). The measurement set up at SALSA is displayed in Fig. 4 (a), which consists of a hexapod stage on which specimens are placed and aligned, a double bent Si monochromator and 2D-PSD He detector. The set up at KOWARI is presented in Fig. 4 (c). In both cases the neutron wavelength was fixed ( $1.64 \text{ \AA}$  at SALSA and  $1.67 \text{ \AA}$  at KOWARI) to measure the Fe  $\alpha$  {211} family of crystallographic planes. This resulted in a diffraction angle near  $90^\circ$  and hence a near

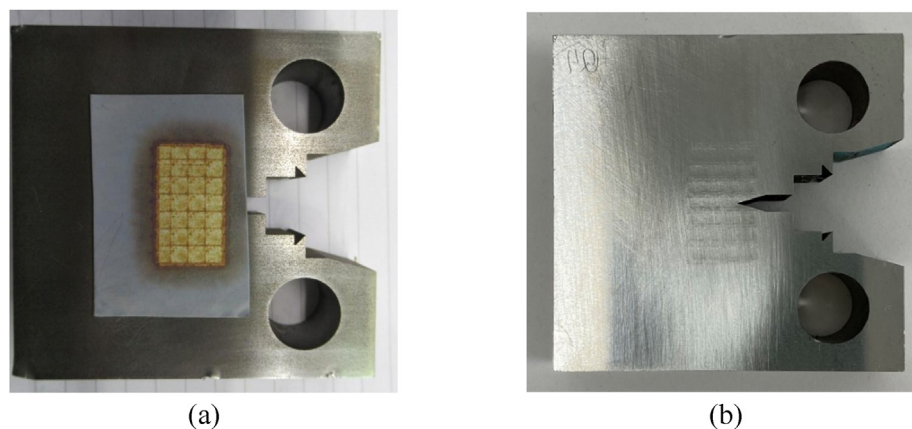
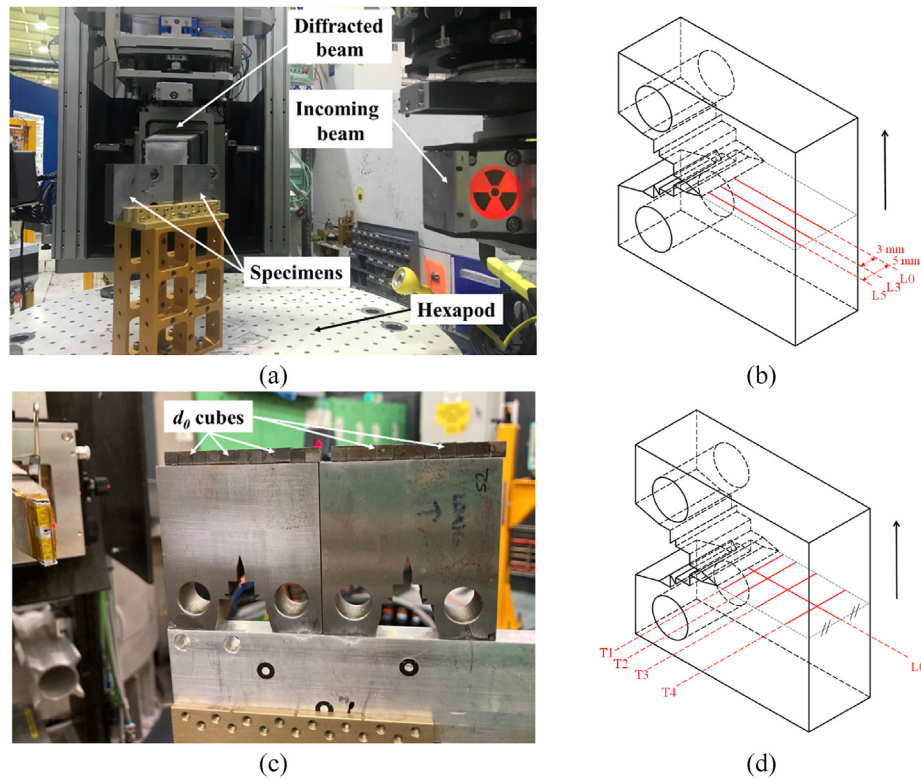


Fig. 3 – An example of the laser shock peening specimen (a) during the surface treatment process, and (b) after the treatment process.



**Fig. 4 – Neutron diffraction (a) test set up at SALS for untreated specimens, and (b) measurement lines with respect to the specimen thickness; (c) KOWARI set up for treated specimens with  $d_0$  cubes measurements and (d) corresponding measurement lines (black arrows indicates the residual stress component of interest).**

cuboid gauge volume. An incoming beam of  $2 \times 2 \text{ mm}^2$  was defined by 2 mm radial collimators on the primary side together with a third radial collimator on the secondary or diffraction side (gauge volume of  $2 \times 2 \times 2 \text{ mm}^3$ ) for these measurements on SALS; and slits system, on both primary and secondary beam, was utilised on KOWARI. Strain mapping in neutron diffraction measurements was performed along the crack propagation line, to capture the residual stress profile ahead of the crack tip along the loading direction of C(T) specimens (i.e. perpendicular to the crack plane). In order to measure the through-thickness residual stress profile in untreated specimens at SALS, the neutron diffraction measurements were conducted along three different lines with the first set of measurements carried out at the mid-thickness (which is shown with line L0 in Fig. 4 (b)) and the other two with 3 mm (L3) and 5 mm (L5) distance from the mid-thickness of the specimen (see Fig. 4 (b)). The mid-thickness measurement L0 was repeated on treated specimens at KOWARI. Additionally, using the gauge volume of  $0.5 \times 0.5 \times 0.5 \text{ mm}^3$ , the through-thickness lines were measured in the specimens: T1, T2, T3 and T4 with 1.5, 5, 10, and 16.5 mm away from the crack tip respectively (Fig. 4 (d)), to examine the symmetry of the residual stresses in treated specimens. The component of stress normal to the crack path, representing the direction of the applied load on C(T) specimens (shown with black arrow in Fig. 4 (b) and (d)), was used in further crack propagation analysis.

In order to assess the stress-free reference value of  $d$  spacing,  $d_0$ , a series of cubes with the dimensions of  $5 \times 5 \times 5 \text{ mm}^3$  were extracted along the crack path from nominally identical specimens without any surface treatment [42]. Different sets of  $d_0$  cubes, corresponding to different specimen locations and orientations extracted from the WAAM wall, were prepared, and measured to minimise the error in neutron diffraction results obtained from each specimen. All  $d_0$  cubes were extracted using the EDM technique to avoid the machining effects on the obtained stress-free values. An example of the cubes extracted for  $d_0$  measurements in two C(T) specimens is illustrated in Fig. 4 (c). The extraction and measurement of  $d_0$  cubes from WAAM build specimens enabled the material and microstructural variations along the crack path to be captured in residual stress measurements [43]. Therefore, the presented residual stress results in this study have higher accuracy with regards to additive manufactured specimens and their potential microstructural gradients compared to alternative  $d_0$  measurement techniques, such as the stress equilibrium or measurement at the corner of the specimen, which are conventionally used for  $d_0$  measurements in relatively homogeneous materials.

During the neutron strain diffraction measurements, the neutron wavelength was kept constant, and the diffraction angle was measured. Subsequently, the lattice parameter  $d$  was measured using the Bragg's law [44]:

$$n\lambda = 2d_{hkl} \sin \theta_{hkl} \quad (1)$$

where  $n$  is a constant,  $\lambda$  is the neutron wavelength,  $d$  is the lattice spacing or the distance between sets of parallel crystallographic planes characterised by the Miller indices  $hkl$ , and  $\theta$  is the scattering angle.

Effectively, the accurate measurements of the distance between similarly oriented planes of atoms can be used as a tool to measure elastic strain. Every change in the lattice spacing ( $\Delta d$ ) represents a residual strain, which can be calculated using the following equation:

$$\varepsilon_{hkl} = \frac{\Delta d_{hkl}}{d_{0,hkl}} = \frac{d_{hkl} - d_{0,hkl}}{d_{0,hkl}} \quad (2)$$

where  $d_0$  is the corresponding stress-free value of lattice spacing, obtained from the extracted cubes, at the point of measurement.

The residual stress in each direction can be calculated from the residual strains using the Hooke's law, which can be described as:

$$\sigma_i = \frac{E}{(1+\nu)(1-2\nu)} [(1-\nu)\varepsilon_i + \nu(\varepsilon_j + \varepsilon_k)] \quad (3)$$

where  $E$  is the elastic Young's modulus and  $\nu$  is Poisson's ratio. The crystallographic values of the elastic modulus and Poisson's ratio used in this study for Fe  $\alpha$  {211} family of crystallographic planes were  $E = 210$  GPa and  $\nu = 0.25$  [45].

#### 4.2. X-ray diffraction method

Upon application of the surface treatment techniques onto the four ER100S-1 specimens, the near surface residual stress measurements were performed, to identify the residual stress profiles at the outer surface of C(T) specimens as a result of the treatment process. For this purpose, diffraction measurements were conducted using laboratory X-ray diffractometers. Phase analysis was carried out using a Malvern Panalytical EMPYREAN diffractometer, enabling the location of diffraction reflections based on which the residual stresses were determined with high precision [46,47]. A copper X-ray tube generating the  $K_{\alpha 1}$  radiation of the wavelength equal to  $\lambda = 1.54 \text{ \AA}$  was used in order to employ the planned phase composition analysis. Detection of the diffracted beam intensity was implemented by the PIXcel1D semiconductor detector with Soller slits  $0.04^\circ$  placed in the path of the diffracted beam. The spot size was  $1 \times 1 \text{ mm}^2$  and the phase composition was measured in  $2\theta$  angular range from  $20^\circ$  to  $152.31^\circ$  in classical Bragg-Brentano geometry. The step of  $2\theta$  angle was  $0.0525^\circ$  and the measurement time at each step was 3600 s.

Similar to the neutron diffraction measurements, surface X-ray diffraction measurements were conducted along the crack path of the specimens starting from the crack tip. The stress component perpendicular to the crack path, which provides the crack driving force, was recorded during the X-ray measurements. An interval of 1 mm distance between the consecutive measurement points was selected for X-ray residual stress experiments. The maximum X-ray penetration depth for the experiments described above was  $37.5 \text{ \mu m}$ .

### 5. Fatigue crack growth testing and analysis

Fatigue crack growth (FCG) tests were conducted on all surface treated C(T) specimens using a 100 kN servo-hydraulic Instron machine under Mode I fracture mechanics loading conditions, in accordance with the ASTM E647 standard [39]. All tests were performed at the room temperature with the load ratio (i.e.,  $P_{min}/P_{max}$ ) of  $R = 0.1$ , where the maximum applied load was  $P_{max} = 10$  kN. The FCG tests were performed using a constant amplitude sinusoidal cyclic waveform with 5 Hz frequency. Prior to FCG testing, all specimens were pre-cracked, under cyclic loading condition, from the initial machined notch of  $a_0 = 17$  mm to approximately 20 mm ( $a_{i,p}/W = 0.4$ ) using the load decreasing approach, introducing infinitely sharp crack tip ahead of the machined notch. During the pre-cracking process, it was ensured that the value of maximum stress intensity factor  $K_{max}$  corresponding to  $P_{max}$  did not exceed the initial  $K_{max}$  in the actual FCG test, so that the FCG results were not influenced by any significant pre-existing plasticity ahead of the initial crack tip.

In order to estimate the instantaneous crack length  $a_i$ , during both pre-cracking and FCG tests, the unloading compliance method was implemented by calibrating and attaching a clip gauge onto the knife edges of the specimen (as shown in Fig. 5). Furthermore, two high resolution cameras were placed on each side of the C(T) specimen to ensure that the crack growth occurred evenly on both sides of the specimen and cross check the estimated values of the crack length obtained from the compliance method. All C(T) specimens were tested until the estimated value of crack length reached 35 mm ( $a_{f,c}/W = 0.7$ ) at the end of the experiment. The FCG test set up is presented in Fig. 5.

During the FCG tests the number of cycles and instantaneous crack lengths, estimated using the compliance technique, were continuously recorded. Subsequently, the FCG rates,  $da/dN$ , were calculated employing a combination of the secant method (for the first and the last three data points), and seven-point incremental polynomial method (for the rest of the data points). The stress intensity factor (SIF) range,  $\Delta K$ , was then computed following the shape function equation presented in Eq. (4) that was developed by Mehmanparast et al. [48] and provides more accurate solutions for the shape

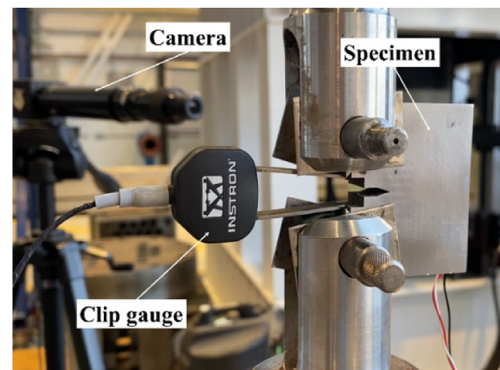


Fig. 5 – Fatigue crack growth test set up.



function in a C(T) specimen for a wider range of crack lengths,  $0.2 \leq a/W \leq 0.7$ , compared to that recommended in the ASTM E647 standard. In Eq. (4),  $\alpha$  is the normalised crack length,  $a/W$ , and  $\Delta P$  is the load range, which is defined as the difference between  $P_{max}$  and  $P_{min}$ .

$$\Delta K = \frac{\Delta P}{BW} \cdot \sqrt{a} \cdot (-372.12\alpha^6 + 1628.60\alpha^5 - 2107.46\alpha^4 + 1304.65\alpha^3 - 391.20\alpha^2 + 54.81\alpha + 7.57) \quad (4)$$

## 6. Experimental results and discussions

### 6.1. FCG test results

Two sets of analyses were conducted on the FCG test data to examine the surface treatment effects on the fatigue performance of WAAM built specimens: based on their orientation and extraction location. The recorded raw data during the FCG tests, which included the crack length,  $a$ , and the number of cycles,  $N$ , were plotted against each other as shown in Fig. 6. Also included in Fig. 6, are the average FCG trends (AV) from nominally identical untreated specimens extracted from ER70S-6 WAAM wall [49] with vertical (70-V-AV) and horizontal (70-H-AV) orientations in Fig. 6 (a), and from top (70-T-AV) and bottom (70-B-AV) of the walls in Fig. 6 (b). Similarly, results obtained from treated samples were compared with the average trends from untreated specimens made with

ER100S-1 steel [50] for different orientations in Fig. 6 (c) and locations in Fig. 6 (d).

The comparison of the crack growth trends in Fig. 6 (a) demonstrates that both surface treatment techniques, LP and R, are effective for life enhancement of ER70S-6 vertical specimens, with surface rolling increasing the test duration by 2.1 times and laser shock peening by 2.5 times compared to the average trend from untreated specimens. On the other hand, for ER70S-6 horizontal specimens the surface treatment techniques were not found beneficial, and both techniques have reduced the test duration on average by around 15% compared to untreated specimens. It is worth noting here, that both rolled specimens, despite of their orientation, showed similar performance. Laser shock peening of ER70S-6 vertical specimen has presented the longest test duration; however, in laser peened horizontal specimen the crack has propagated 1.5 times quicker than in untreated horizontal specimens. Evaluation of the FCG results based on the specimen location in ER70S-6 WAAM wall (Fig. 6 (b)) shows that two rolled specimens extracted from the top of the wall have slightly improved test duration. Laser shock peening has demonstrated an increase in the test duration for one bottom specimen by 24%, and reduction by 18% for the second bottom specimen. It can be concluded that regardless of the comparison method (by orientation or location), the best performance for ER70S-6 wall was shown by laser peened specimen 70-VB-LP, though using the same surface treatment technique on 70-HB-LP specimen only worsens the fatigue life.

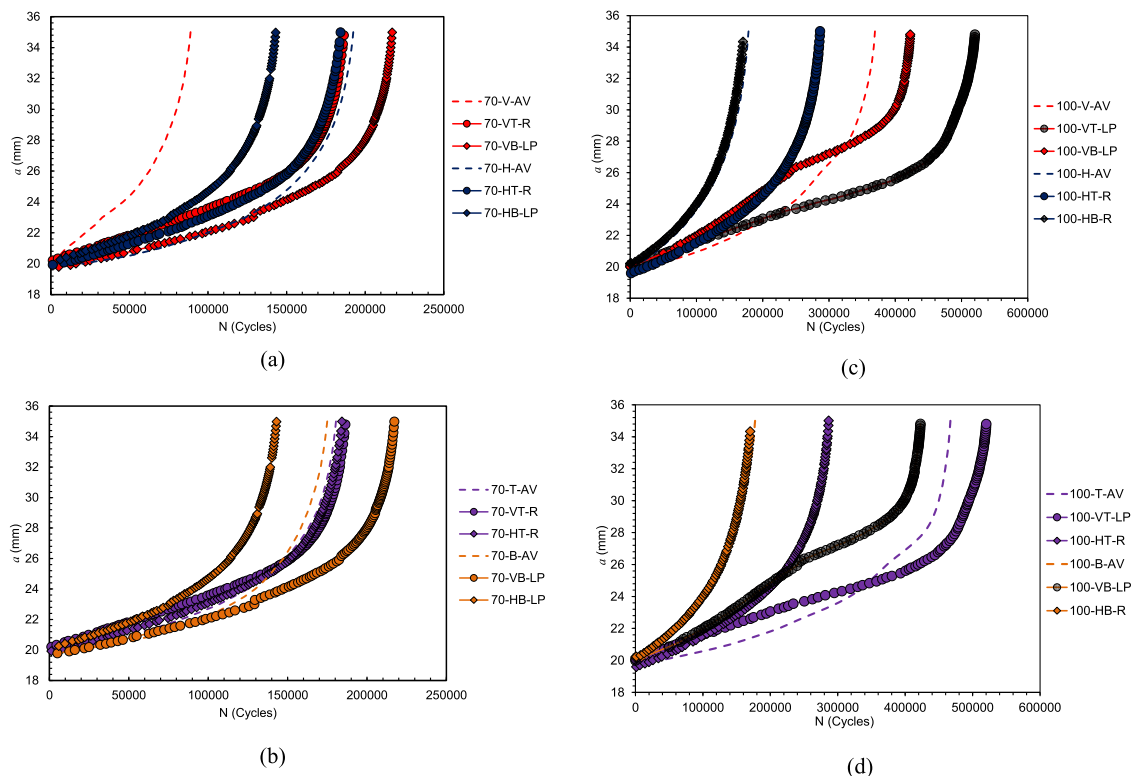


Fig. 6 – Comparison of FCG trends for surface treated WAAM specimens with average FCG trends from untreated specimens for (a–b) ER70S-6, and (c–d) ER100S-1 specimens.



Analysing the FCG data for ER100S-1 specimens with different orientations (Fig. 6 (c)), it can be seen that laser peening surface treatment increased the fatigue life in vertical specimens on average by 27%. The fatigue life enhancement was also observed in one rolled horizontal specimen, improving the test duration by 1.6 times. However, for the second horizontal specimen, 100-HB-R, surface treatment application was not beneficial, and the results are found to be very similar to the average results for untreated specimens. Further comparison of the FCG results for different extraction locations of ER100S-1 specimens (Fig. 6 (d)) demonstrates that laser peening was a more effective surface treatment technique for both top and bottom specimens, increasing the number of cycles by 1.1 and 2.4 times, respectively. However, rolling not only did not improve the test duration but worsened the results for both extraction locations. It should be noted here, that for both examined materials, the worst results were presented by horizontal specimens extracted from the bottom of WAAM walls, regardless of the applied surface treatment method. Thus, the best life enhancement was achieved by laser peening technique applied on vertical bottom specimen 70-VB-LP for ER70S-6 steel and on vertical top specimen 100-VT-LP for ER100S-1.

The FCG rates were obtained from the tests by calculating  $da/dN$  and then correlated with the SIF range,  $\Delta K$ , the results are shown in Fig. 7. Two sets of analyses were also carried out on the FCG rates data to investigate the sensitivity of the specimen orientation and location to the surface treatment. In Fig. 7, the results obtained from this study on surface treated specimens are compared with the FCG data on nominally identical untreated specimens [49,50], for which the mean line

(MN) was plotted along with mean  $\pm 2$  standard deviation (SD) trends.

In Fig. 7 (a) it can be seen that the FCG rates for surface treated ER70S-6 vertical specimens are up to 2 times lower than the mean-2SD line from untreated specimens for the SIF range of up to  $\Delta K \approx 30.5 \text{ MPa}\sqrt{\text{m}}$ , which corresponds to the crack extension of approximately  $\Delta a = 8 \text{ mm}$  – the length of the surface treated region. At higher  $\Delta K$  values, the FCG rates for vertical specimens fluctuate about the mean line, but do not exceed the mean+2SD line for untreated specimens. The vertical surface treated specimens present the lowest trends. The FCG trend for rolled horizontal specimen is found similar to the vertical specimens; however, it is crossing the mean-2SD line for horizontal untreated specimens at  $\Delta K \approx 25.4 \text{ MPa}\sqrt{\text{m}}$ , which corresponds to the crack extension of approximately  $\Delta a = 6 \text{ mm}$ , then it falls upon the mean line until the end of the test. As for the laser peened specimen, which showed the shortest test duration among the treated specimens, 70-HB-LP, the FCG rates fluctuate between the mean  $\pm 2$ SD lines throughout the test, without showing any deterioration in the rates.

Comparison of the results based on their extraction locations for ER70S-6 specimens in Fig. 7 (b) shows FCG rate enhancement (below mean-2SD line) for rolled top specimens at a range of  $\Delta K$  values up to approximately  $25.5 \text{ MPa}\sqrt{\text{m}}$  (corresponding to  $\Delta a = 5.8 \text{ mm}$ ). The laser peened vertical bottom specimen, 70-VB-LP, represents the lowest FCG rates at the beginning of the test (at low  $\Delta K$  values), showing considerable improvement in the crack growth rates, with the lower FCG trend at a wide range of SIF of up to  $\Delta K = 31 \text{ MPa}\sqrt{\text{m}}$ , corresponding to crack extension of  $\Delta a = 8.7 \text{ mm}$ . Then it

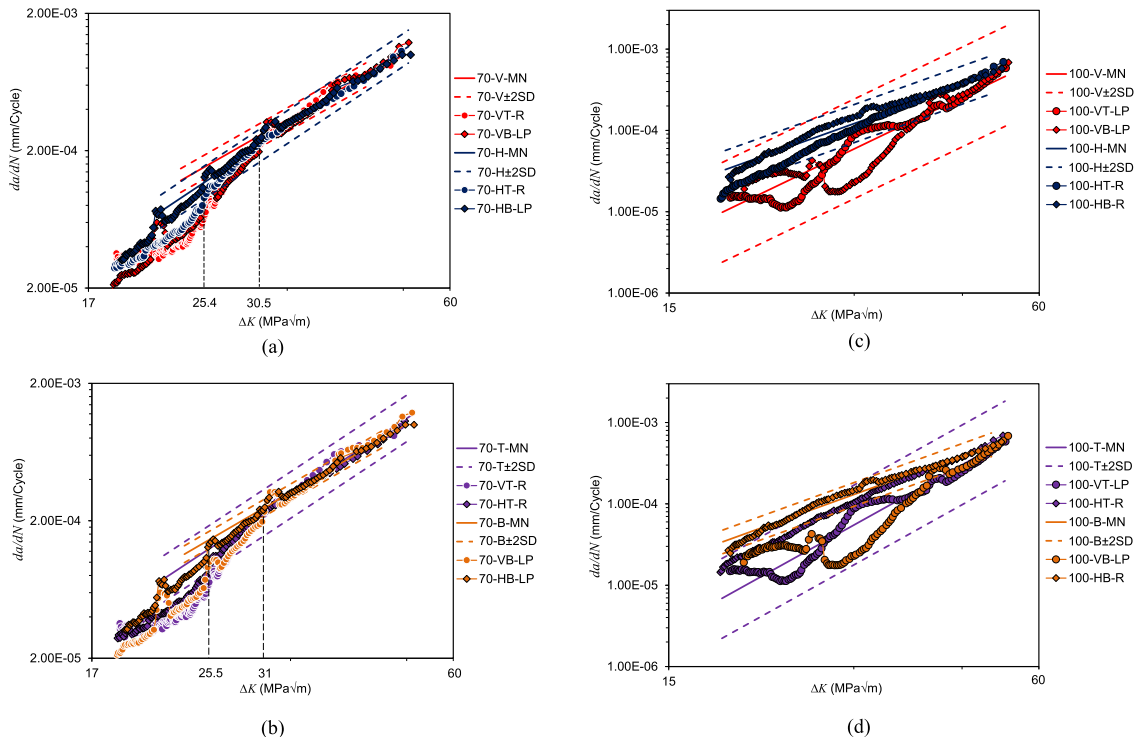


Fig. 7 – Comparison of the FCG test results for surface treated specimens with average FCG trends from untreated specimens for (a–b) ER70S-6, and (c–d) ER100S-1 specimens.

crosses the lower bound for untreated specimens and fluctuates along the mean line until the end of the test. On the other hand, another laser peened specimen from the bottom of the wall, 70-HB-LP, is showing the highest FCG trends at lower values of SIF and crossing the mean-2SD line at  $\Delta K = 25.5 \text{ MPa}\sqrt{\text{m}}$  (corresponding to  $\Delta a = 5.8 \text{ mm}$ ). All four test results converge midway through the test. It can be concluded here that both surface treatment techniques are effective on ER70S-6 specimens, decreasing the FCG rates in the beginning of the test (while the crack grows through the treated area) and converging to the mean FCG trend from untreated specimens by the end of the test.

Evaluation of the FCG rates for ER100S-1 specimens with different orientations from Fig. 7 (c) shows that the effect of surface treatment on this material is less pronounced compared with ER70S-6, as the trends for the treated specimens do not go beyond the mean±2SD lines, regardless of their orientation and selected surface treatment technique. However, an important point that can be noted here is that the results for vertical specimens are mostly located in the lower half between the mean and mean-2SD lines, indicating positive effect of laser peening treatment. Similar behaviour is observed for rolled horizontal specimen 100-HT-R, which starts at the mean-2SD line of horizontal untreated specimens and progresses towards the mean line by the end of the test. However, 100-HB-R specimen which had the shortest test duration among all experiments conducted in this research, presents the highest FCG rates compared to other specimens and its trend is mostly located between the mean and mean + 2SD lines, confirming that no improvement was achieved by rolling this specimen.

From Fig. 7 (d), which demonstrates a comparison of FCG rates for ER100S-1 specimens based on their extraction location, it can be seen that the FCG trend for laser peened 100-VB-LP specimen extracted from the bottom of WAAM wall is lower than mean-2SD line for the bottom untreated specimens throughout the test and presents the lowest FCG rates among all four tested specimens. This trend is the only example of sufficient FCG rate improvement achieved by surface treatment on ER100S-1 specimens as its trend starts and stays below the mean-2SD line for untreated specimens throughout the test. The trend with the highest FCG rates belongs to rolled specimen from the bottom of the wall 100-HB-R, though it fluctuates between the mean ± 2SD lines during the test. No life enhancement effect is seen for the top laser peened specimen 100-VT-LP, the results for which fluctuates about the mean line. The worst FCG performance compared to the mean line from untreated specimens is seen for top rolled specimen 100-HT-R, the trend for which is located in the upper half between the mean and upper bounds for untreated specimens. Thus, it can be concluded here that surface rolling is a less effective surface treatment technique compared to laser shock peening for ER100S-1 under the examined rolling parameters and testing conditions. Moreover, it should be noted here that regardless of the material and applied surface treatment technique, horizontal specimen extracted from the bottom of WAAM wall is showing the highest FCG rates and shortest test duration. Considering that only four specimens were surface treated and then tested for FCG in the present study, more tests need to be conducted in

future work to confirm the provisional results presented in this paper and assess the level of scatter for each specimen orientation and location.

### 6.2. Residual stress measurement results

The residual stress measurements, before and after surface treatment, for ER100S-1 specimens with the longest (100-VT-LP) and shortest test durations (100-HB-R) are presented in Fig. 8, showing the component of stress normal to the crack path (Fig. 4 (c) and (d)). As mentioned in Section 4, neutron diffraction measurements were performed on untreated and treated specimens, with additional X-ray measurements in the near surface region of treated specimens. The error bars have shown minor variation within 10–20 MPa and were not included in the residual stress trends. It can be observed in Fig. 8 (a) that 100-VT specimen had a pronounced state of tensile residual stresses ahead of the crack tip before any surface treatment, with a peak value of around 400 MPa within the bulk. As seen in Fig. 8 (a), through thickness characterisation revealed generally similar residual stress profiles for L0, L3 and L5 at the distance between 0 to approximately 15 mm from the crack tip while a slightly higher residual stress value was identified for lower penetration depths from the specimen surface. However, as seen from the near surface X-ray results, laser shock peening introduced a significant compressive residual stress of around –260 MPa at the crack tip and further compressive stresses in the region between 1.5

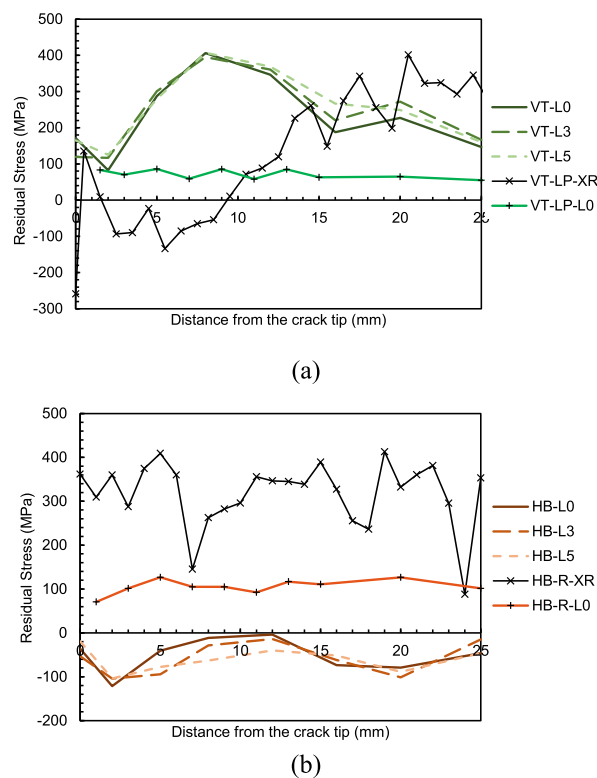


**Fig. 8 – Residual stress distribution in ER100S-1 specimens before and after surface treatment (a) 100-VT specimen before and after laser shock peening, (b) 100-HB specimen before and after surface rolling.**

and 9.5 mm from the crack tip, which corresponds to the region where the laser peening treatment was applied (see Section 3.2), shifting the peak of the tensile residual stresses further away from the crack tip. The mid-thickness ND measurement L0 in treated VT-LP specimen shows that application of LP at the surface of the specimen subsequently reduces the tensile residual stresses in the middle of the specimen, which becomes almost constant along the crack path, with average value of 70 MPa. The residual stress results are in excellent agreement with the FCG behaviour of 100-VT specimen observed in Fig. 6 (c–d). Where an increased fatigue life was observed in the surface treated specimen with slowed down crack propagation rate in the peened region, caused by beneficial compressive residual stresses, followed by accelerated cracking behaviour beyond the peened area, caused by detrimental tensile residual stresses. Fig. 8 (b) shows an opposite residual stress transition trend in 100-HB specimen before and after surface treatment. This specimen initially had a compressive residual stress field along the crack path within the bulk, reaching up to  $-100$  MPa with no significant gradients across thickness at L0, L3 and L5. However, as shown by X-ray results, the surface rolling treatment introduced damaging tensile residual stresses on the surface with amplitude of between 100 and 400 MPa on the full length of the crack path. The ND measurements in mid-thickness of the treated specimen HB-R also detect the introduced tensile stresses along the crack path, with minor fluctuations and the average value of 105 MPa. This led to the shortest fatigue life discovered among all specimens in Fig. 6 (c–d) and the highest FCG rates in Fig. 7 (c–d). It is worth noting here, that minor fluctuations in the peak residual stresses measured before surface treatment application at L0, L3 and L5 are seen for both specimens, indicating generally lower peak stress values at the mid-thickness, which gradually grow towards the surface of the specimen. The observed through-thickness residual stress distribution field is in good agreement with previous studies [51,52].

Comparison of Fig. 8 (a) and (b) demonstrates that the residual stress before application of any surface treatment is lower in specimens extracted from the bottom of the WAAM wall. This can be associated with a higher number of thermal cycles applied on the layers deposited at the bottom of the WAAM wall which would relax the residual stresses in this region, compared to the top layers which are subjected to a lower number of thermal cycles. Moreover, the residual stress measurement results on ER100S-1 specimens show that laser shock peening is an effective surface treatment technique to remove the detrimental tensile residual stresses at the top region of the WAAM wall, hence increasing the fatigue life and decelerating the FCG rates, while the bottom region of the WAAM wall exhibits a better state of residual stress, owing to an enhanced fatigue performance, without applying any surface rolling treatment.

It should be noted that according to the study by Gornyaev et al. [53] during the surface rolling process on WAAM built components, a relatively high tensile residual stress zone can be developed behind the roller, in the treated region and near the outer surface of the component, which is due to the non-uniform distribution of plastic deformation. Also, it is known that laser shock peening is capable of introducing

significant levels of compressive residual stresses due to relatively uniform surface hardening effects [54,55]. This shows that the conclusions from similar studies on the WAAM built components in the literature are consistent with the observations from this study.

The through-thickness residual stress distribution of treated vertical ER100S-1 specimens is presented in Fig. 9 (a) for laser peened specimen and (b) for rolled specimen, showing the component of stress normal to the crack path (Fig. 4 (c) and (d)). From these figures it can be seen that the residual stress trends are asymmetrical with respect to the mid-thickness plane of the specimens regardless of the surface treatment technique. The difference between stress values on the opposite sides of the specimen, 0.95 mm away from the surface, is up to 8 times for the laser peened

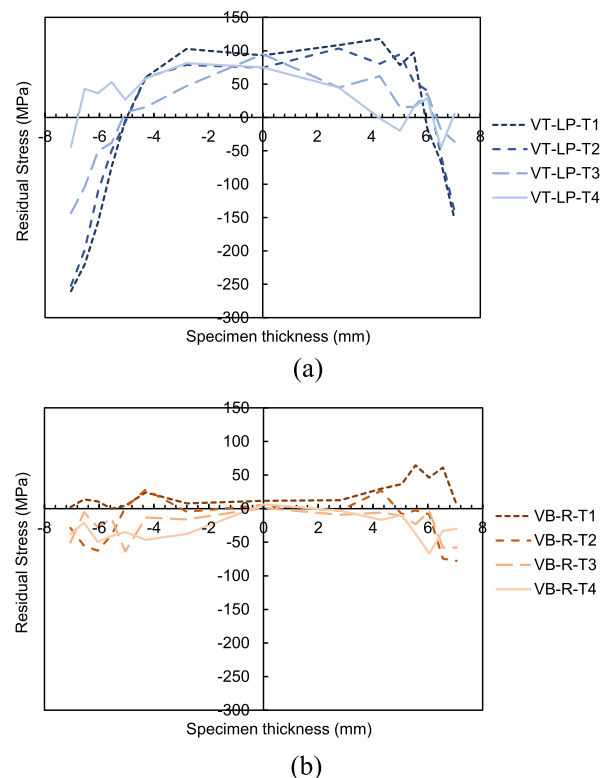


**Fig. 9 – Through-thickness residual stress distribution in treated areas of ER100S-1 vertical specimens (a) laser peened and (b) rolled. (Specimen thickness is 16 mm).**

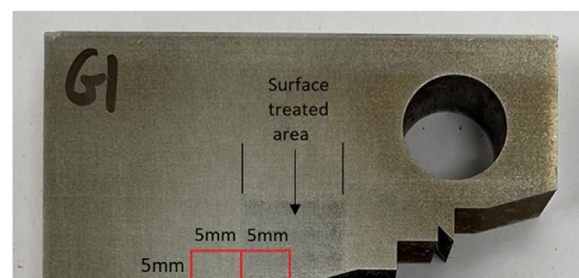


**Fig. 10 – An example of the coupon extraction region on a surface treated sample.**



specimen, whereas for the rolled specimen is up to 2.7 times. Moreover, it can be seen from the trends that application of LP surface treatment induces higher compressive stresses near specimen surface region, which gradually reduce within first 1.5–2 mm from the surface, and then balance with increasing

tensile stresses towards the middle of the specimen. The trend for rolled specimen is not as clear and shows fluctuations in stress throughout the specimen thickness, with low tensile stress between 0 and 13 MPa in the middle of the specimen. It is also seen that T1 measurement line (1.5 mm

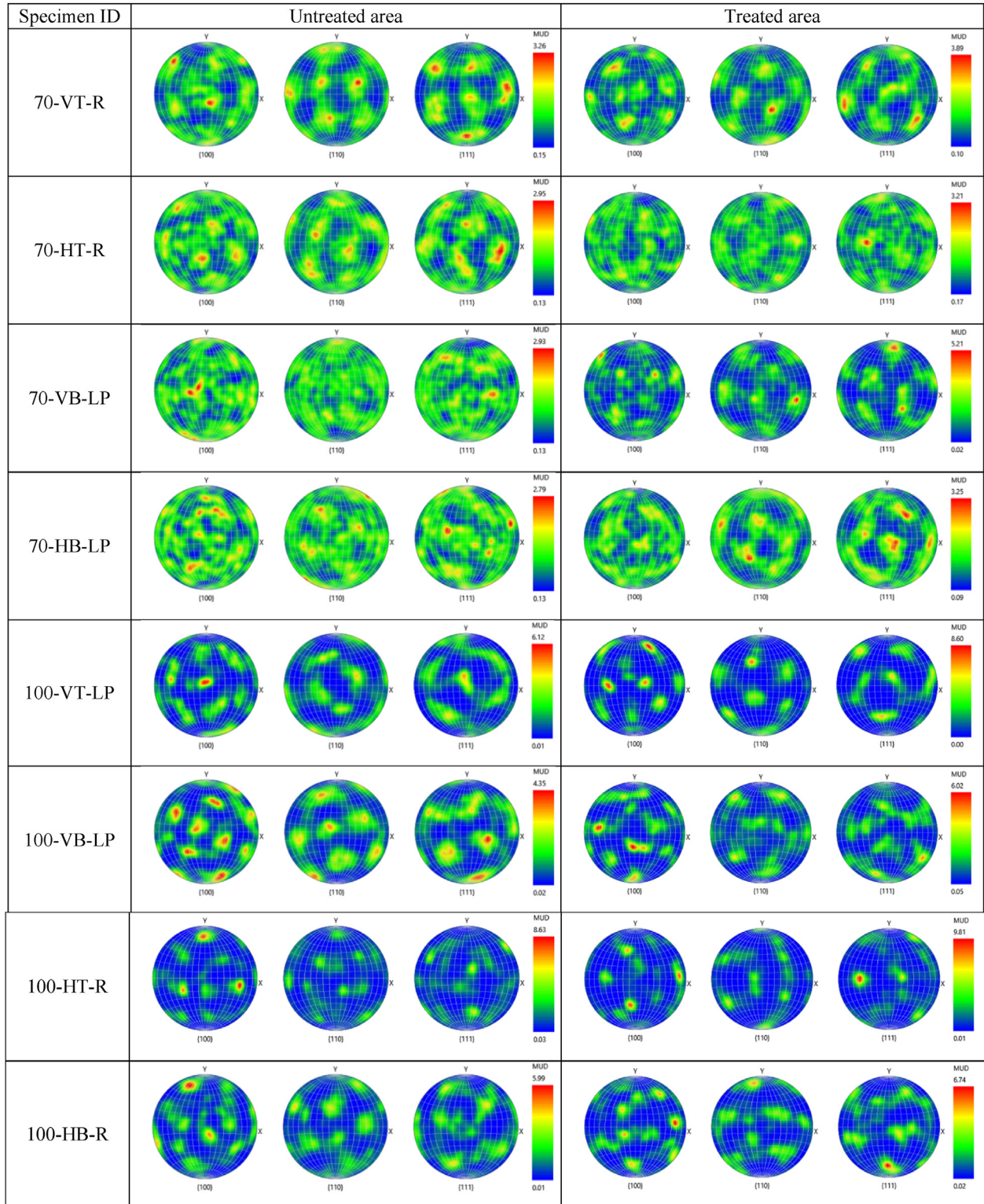


Fig. 11 – Comparison of the pole figures in untreated and treated regions in WAAM built specimens made of ER70S-6 and ER100S-1.



away from the crack tip) in rolled specimen shows absence of compressive residual stresses throughout the thickness of the specimen. The maximum compressive stress near the surface for LP specimen is 3.4 times higher than for rolled specimen, confirming higher efficiency of laser peening surface treatment technique on ER100S-1 WAAM built specimens. Further seen in the results is that the maximum tensile stress value in the middle of the specimen is 7.7 times higher in LP specimen than in rolled one. Asymmetrical residual stress distribution in treated specimens can be due to the selected procedure for the surface treatment application, which was not conducted simultaneously on both specimen sides, but instead was done on one side at a time.

### 6.3. Microstructural analysis

Upon completion of the FCG tests, all eight specimens were broken-open into halves by initially soaking them in liquid nitrogen for a few minutes, to minimise the plastic deformation during fracture, and then pulling them apart using the servo-hydraulic machine. A  $10 \times 5 \times 5 \text{ mm}^3$  coupon was extracted from each C(T) specimen using the EDM technique in such a way that along the 10 mm length, 5 mm was taken from the treated region and 5 mm from the untreated surface (see Fig. 10). The coupons were mounted in a conductive resin, ground and polished to  $1 \mu\text{m}$  surface finish, with final polishing conducted using colloidal silica suspension. Electron Backscatter Diffraction (EBSD) measurements were performed on the coupons using an Oxford Instruments Symmetry with accelerating voltage of 20 keV, beam current of 5 nA, field of view of  $300 \mu\text{m}$  and step size of  $0.7 \mu\text{m}$ . The pole figures obtained from the untreated and treated regions of the specimens are presented in Fig. 11. Furthermore, the texture indices were measured at the untreated and treated regions in each coupon and compared with each other in Table 3 and Fig. 12.

Analysis of the pole figures in Fig. 11 shows that the surface treated regions have a higher texture compared to the untreated regions. Moreover, as seen in Fig. 11 the maximum values of the Multiple of Uniform Density (MUD) are higher in the regions with the surface treatment. Comparison of the pole figures between the two materials shows that the untreated ER100S-1 has considerably higher texture compared to the untreated ER70S-6 material. A quantitative comparison of the texture indices in Table 3 also verifies that both surface treatment techniques (i.e. surface rolling and laser shock peening) introduced a higher texture into the WAAM built specimens; however, applying the laser shock peening has increased the texture index on average by 22.5%, whereas for rolling it is 8.3%. Another observation that can be made from Fig. 12 is that the initial texture index for untreated specimens is higher in vertical specimens made of ER70S-6, compared to the horizontal samples, and for top specimens made of ER100S-1 material, compared to the bottom samples. This agrees with the general observation from the FCG analysis that ER70S-6 WAAM specimens were more sensitive to the extraction orientation [49], while ER100S-1 specimens showed more sensitivity to the extraction location [50]. Finally seen in Table 3 and Fig. 12 is that for both materials examined in this study the jumps in the texture indices from the untreated

**Table 3 – Comparison of the texture indices in untreated and treated regions.**

Specimen ID	Texture Index		
	Untreated	Treated	Difference
70-VT-R	1.29	1.43	11%
70-HT-R	1.02	1.05	3%
70-VB-LP	1.35	1.82	35%
70-HB-LP	1.04	1.10	6%
100-VT-LP	2.30	2.88	25%
100-VB-LP	1.76	2.19	24%
100-HT-R	2.60	2.89	11%
100-HB-R	2.17	2.34	8%

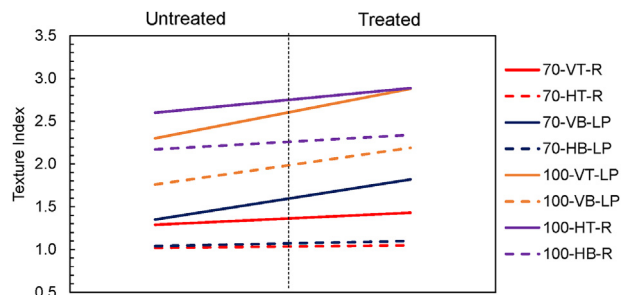


**Fig. 12 – Visual representation of the change in the texture indexes from the untreated region (on the left-hand side) to the treated region (on the right-hand side).**

region to the treated region were found to be generally higher by applying the laser shock peening treatment compared to the surface rolling treatment. It can be seen that the texture index after the surface treatment is on average 2.7 times higher in the laser shock peened regions than in the rolled areas.

The inverse pole figures in Z direction (IPF-Z) were captured for both untreated and treated specimen areas and are shown in Fig. 13. As seen in this figure, larger grains are observed in ER70S-6 specimens compared to ER100S-1 specimens, which implies higher ductility and toughness parameters and lower strength for ER70S-6 WAAM built components [38]. There is no major grain refinement visible for both materials after applying the surface treatments using the considered treatment parameters. The grain size distribution analysis demonstrated that the total number of grains for ER70S-6 has increased on average by 10% for rolled and 25% for laser shock peened specimens, reducing the mean area of grains by 3% and 13%, respectively. For ER100S-1, the total number of grains raised only by 4% for rolled and 16% for laser shock peened specimens, refining the mean grain area by 15% and 7%, respectively. Finally seen in Fig. 13 is that the cracking mode in FCG tests performed the WAAM built specimens made of both materials was transgranular.

Finally, further microstructural analysis was conducted to evaluate the deformation mechanism through residual strain distribution and the results in form of the kernel average misorientation (KAM) maps are shown in Fig. 14. In this analysis the same step size and settings were used to capture the residual strain distribution maps, therefore the obtained

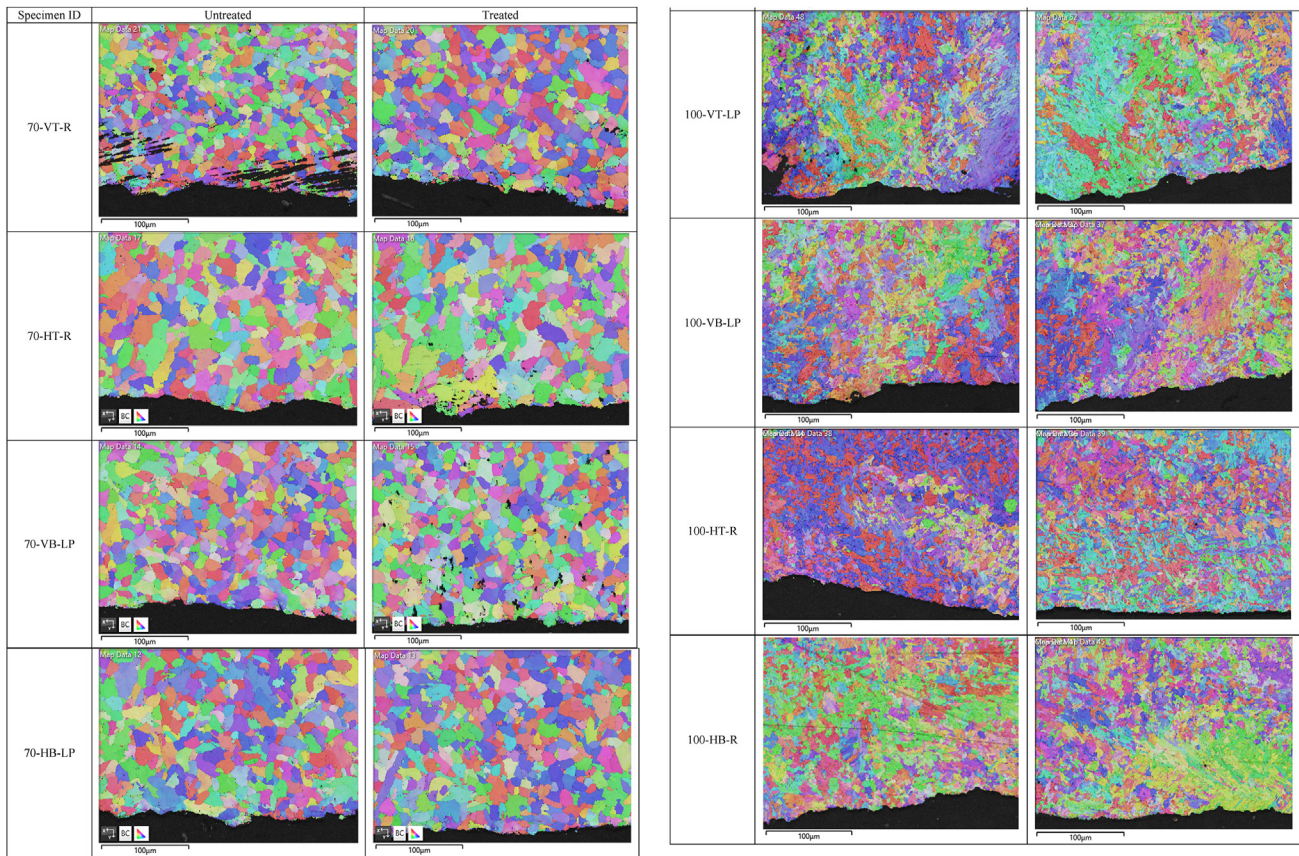


**Fig. 13 – Inverse pole figures captured from the untreated and treated regions of WAAM built specimens.**

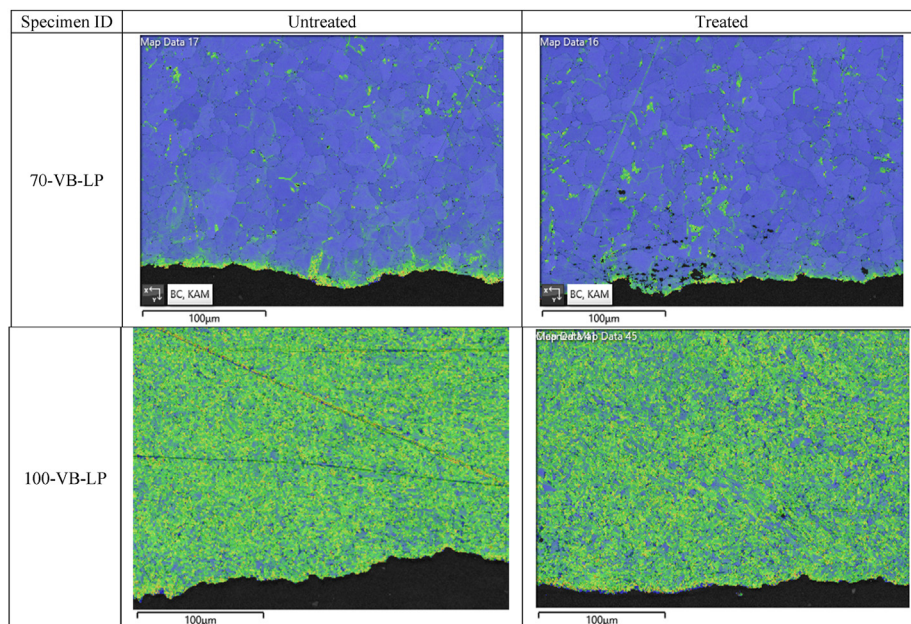


**Fig. 14 – Residual strain analysis for WAAM built specimens made of ER70S-6 and ER100S-1.**

results are directly comparable with each other [56]. It can be seen in Fig. 14 that the largest deformation, hence a higher level of residual strain, was found along the crack path in ER70S-6 specimens. For ER100S-1 specimens it can be clearly

observed in Fig. 14 that most of deformation in this material is located at the surface of the examined coupon, which is visible by the dominantly green colour throughout the examined area. Very little difference in residual strains was



found between the untreated and treated regions in each specimen.

## 7. Conclusions

In this study the effects of laser shock peening and surface rolling treatments on the FCG behaviour were comprehensively examined, along with the residual stress distribution and material texture of WAAM built low carbon steel components. The following conclusions can be drawn based on the obtained results from this work.

- For ER70S-6 WAAM built components, both surface treatment techniques have been found to enhance the fatigue performance by reducing the FCG rates in the surface treated area compared to the untreated material.
- For both materials, the laser shock peening technique resulted in the longest fatigue lives compared to the untreated samples. The longest test durations in laser peened specimens were observed in the vertical specimens extracted from the bottom of ER70S-6 and the top of ER100S-1 WAAM walls.
- Application of rolling surface treatment, using the same parameters on both materials, was found to be inefficient for ER100S-1 specimens and resulting in a shorter fatigue life and higher FCG rates compared to the untreated material.
- The surface rolling treatment introduces high residual stresses in the near surface region of ER100S-1 specimens, which resulted in deterioration of FCG performance, whereas laser shock peening induced significant level of compressive residual stresses which were beneficial for fatigue performance and results in lower FCG rates.
- The residual stress measurements through-thickness of treated specimens showed small asymmetrical stress distribution with respect to the mid-thickness plane, which can be due to non-symmetrical application of surface treatment techniques.
- The texture was found to increase by applying both surface treatment techniques; however, for laser shock peened specimens the texture index was found on average 2.7 times higher than the rolled specimens. Moreover, untreated specimens made of ER100S-1 material exhibited a higher texture compared to untreated ER70S-6 specimens.
- ER100S-1 has finer grains compared to ER70S-6 specimens while the cracking mode in both materials was found to be transgranular under fatigue loading conditions.
- A larger amount of residual strain was observed throughout ER100S-1 WAAM specimens, whereas in ER70S-6 specimens the highest residual strains were concentrated along the crack path.
- Repeat tests are required in future work to evaluate the level of scatter for each surface treated specimen extraction location and orientation. Moreover, additional ND measurements need to be conducted to analyse the RS states in all surface treated specimens.

## Declaration of competing interest

The authors declare that they have no known competing financial interests or personal relationships that could have appeared to influence the work reported in this paper.

## Acknowledgements

This work was supported by grant EP/L016303/1 for Cranfield, Oxford, and Strathclyde Universities Centre for Doctoral Training in Renewable Energy Marine Structures – REMS CDT (<http://www.rems-cdt.ac.uk/>) from the UK Engineering and Physical Sciences Research Council (EPSRC). The authors would like to thank ILL-France for provision of the neutron beamtime for residual stress measurements under <https://doi.ill.fr/10.5291/ILL-DATA.1-02-292> and ANSTO (Proposal 13422).

## REFERENCES

- [1] Kumar D, Idapalapati S, Wang W, Narasimalu S. Effect of surface mechanical treatments on the microstructure-property-performance of engineering alloys. *Mater* 2019;429–36.
- [2] Ersdal, G., Sharp, J. V. & Stacey, A. Ageing and life extension of offshore structures: the challenge of managing structural integrity. Available at: [https://books.google.no/books?id=tzB6DwAAQBAJ&pg=PA162&lpg=PA162&dq=grinding+life+extension+steels&source=bl&ots=mi7WNDonqm&sig=ACfU3U0IKLdC3UtdrW3JZXUPNkGfC2eLQ&hl=en&sa=X&ved=2ahUKEwi4mpzh6sf3AhWuS\\_EDHTA-BQ4Q6AF6BAGPEAM#v=onepage&q=grinding life extens.](https://books.google.no/books?id=tzB6DwAAQBAJ&pg=PA162&lpg=PA162&dq=grinding+life+extension+steels&source=bl&ots=mi7WNDonqm&sig=ACfU3U0IKLdC3UtdrW3JZXUPNkGfC2eLQ&hl=en&sa=X&ved=2ahUKEwi4mpzh6sf3AhWuS_EDHTA-BQ4Q6AF6BAGPEAM#v=onepage&q=grinding life extens.) (Accessed: 5th May 2022).
- [3] Luong H, Hill MR. The effects of laser peening and shot peening on high cycle fatigue in 7050-T7451 aluminum alloy. *Mater Sci Eng, A* 2010;527:699–707.
- [4] Gujba AK, Medraj M. Laser peening process and its impact on materials properties in comparison with shot peening and ultrasonic impact peening. *Mater* 2014;7:7925–74.
- [5] Gao YK, Wu XR. Experimental investigation and fatigue life prediction for 7475-T7351 aluminum alloy with and without shot peening-induced residual stresses. *Acta Mater* 2011;59:3737–47.
- [6] Wang Z, Jiang C, Gan X, Chen Y, Ji V. Influence of shot peening on the fatigue life of laser hardened 17-4PH steel. *Int J Fatig* 2011;33:549–56.
- [7] Zhang P, Lindemann J. Influence of shot peening on high cycle fatigue properties of the high-strength wrought magnesium alloy AZ80. *Scripta Mater* 2005;52:485–90.
- [8] Hatamleh O, Lyons J, Forman R. Laser and shot peening effects on fatigue crack growth in friction stir welded 7075-T7351 aluminum alloy joints. *Int J Fatig* 2007;29:421–34.
- [9] Hatamleh O. A comprehensive investigation on the effects of laser and shot peening on fatigue crack growth in friction stir welded AA 2195 joints. *Int J Fatig* 2009;31:974–88.
- [10] Ganesh P, Sundar R, Kumar H, Kaul R, Ranganathan K, Hedaoop, et al. Studies on laser peening of spring steel for automotive applications. *Opt Laser Eng* 2012;50:678–86.
- [11] Kloos KH, Fuchsbaue B, Adelman J. Fatigue properties of specimens similar to components deep rolled under optimized conditions. *Int J Fatig* 1987;9:35–42.

- [12] Altenberger I, Nalla RK, Sano Y, Wagner L, Ritchie RO. On the effect of deep-rolling and laser-peening on the stress-controlled low- and high-cycle fatigue behavior of Ti–6Al–4V at elevated temperatures up to 550 °C. *Int J Fatig* 2012;44:292–302.
- [13] Wong CC, Hartawan A, Teo WK. Deep cold rolling of features on aero-engine components. *Procedia CIRP* 2014;13:350–4.
- [14] Nalla RK, Altenberger I, Noster U, Liu GY, Scholtes B, Ritchie RO. On the influence of mechanical surface treatments—deep rolling and laser shock peening—on the fatigue behavior of Ti–6Al–4V at ambient and elevated temperatures. *Mater Sci Eng, A* 2003;355:216–30.
- [15] Tsuji N, Tanaka S, Takasugi T. Effect of combined plasma-carburizing and deep-rolling on notch fatigue property of Ti-6Al-4V alloy. *Mater Sci Eng, A* 2009;499:482–8.
- [16] Feldmann G, Wong CC, Wei W, Haubold T. Application of vibropeening on aero – engine component. *Procedia CIRP* 2014;13:423–8.
- [17] Rodrigues TA, Duarte V, Miranda RM, Santos TG, Oliveira JP. Current status and perspectives on wire and Arc Additive manufacturing (WAAM). *Mater* 2019;12:1121.
- [18] Cunningham CR, Flynn JM, Shokrani A, Dhokia V, Newman ST. Invited review article: strategies and processes for high quality wire arc additive manufacturing. *Addit Manuf* 2018;22:672–86.
- [19] Dong P. Residual stresses and distortions in welded structures: a perspective for engineering applications. *Sci Technol Weld Join* 2013;389–98. <https://doi.org/10.1179/174329305X29465> 10.
- [20] Dong P, Brust FW. Welding residual stresses and effects on fracture in pressure vessel and piping components: a millennium review and beyond. *J Pressure Vessel Technol* 2000;122:329–38.
- [21] Webster GA, Ezeilo AN. Residual stress distributions and their influence on fatigue lifetimes. *Int J Fatig* 2001;23:375–83.
- [22] Rauch M, Hascoet J. Improving additive manufactured surfaces properties with post processing techniques. 2021.
- [23] McAndrew AR, Alvarez Rosales M, Colegrove PA, Hönnige JR, Ho A, Fayolle R, et al. Interpass rolling of Ti-6Al-4V wire + arc additively manufactured features for microstructural refinement. *Addit Manuf* 2018;21:340–9.
- [24] Colegrove PA, Donoghue J, Martina F, Gu J, Prangnell P, Hönnige J. Application of bulk deformation methods for microstructural and material property improvement and residual stress and distortion control in additively manufactured components. *Scripta Mater* 2017;135:111–8.
- [25] Colegrove PA, Coules HE, Fairman J, Martina F, Kashoob T, Mamash H, et al. Microstructure and residual stress improvement in wire and arc additively manufactured parts through high-pressure rolling. *J Mater Process Technol* 2013;213:1782–91.
- [26] Hönnige JR, Colegrove PA, Ganguly S, Eimer E, Kabra S, Williams S. Control of residual stress and distortion in aluminium wire + arc additive manufacture with rolling. *Addit Manuf* 2018;22:775–83.
- [27] Saboori A, Piscopo G, Lai M, Salmi A, Biamino S. An investigation on the effect of deposition pattern on the microstructure, mechanical properties and residual stress of 316L produced by Directed Energy Deposition. *Mater Sci Eng, A* 2020;780.
- [28] Martina F, Roy MJ, Szost BA, Terzi S, Colegrove PA, Williams SW, et al. Residual stress of as-deposited and rolled wire+arc additive manufacturing Ti–6Al–4V components. *Mater Sci Technol* 2016;32:1439–48.
- [29] Abrão AM, Denkena B, Breidenstein B, Mörke T. Surface and subsurface alterations induced by deep rolling of hardened AISI 1060 steel. *Prod Eng* 2014;8:551–8.
- [30] Munther M, Martin T, Tajyar A, Hackel L, Beheshti A, Davami K. Laser shock peening and its effects on microstructure and properties of additively manufactured metal alloys: a review. *Eng. Res. Express* 2020;2.
- [31] Sun R, Li L, Zhu Y, Guo W, Peng P, Cong B, et al. Microstructure, residual stress and tensile properties control of wire-arc additive manufactured 2319 aluminum alloy with laser shock peening. *J Alloys Compd* 2018;747:255–65.
- [32] Chi J, Cai Z, Wan Z, Zhang H, Chen Z, Li L, et al. Effects of heat treatment combined with laser shock peening on wire and arc additive manufactured Ti17 titanium alloy: microstructures, residual stress and mechanical properties. *Surf Coating Technol* 2020;396:125908.
- [33] Luo S, He W, Chen K, Nie X, Zhou L, Li Y. Regain the fatigue strength of laser additive manufactured Ti alloy via laser shock peening. *J Alloys Compd* 2018;750:626–35.
- [34] Manikandan M, Mani Prabu SS, Jayachandran S, Akash K, Palani IA, Karunakaran KP. Influence of laser shock peening on Wire Arc Additive manufactured low carbon steel. 2019. p. 509–16. [https://doi.org/10.1007/978-981-32-9425-7\\_45](https://doi.org/10.1007/978-981-32-9425-7_45).
- [35] Lincoln Electric Company, T. lincoln ® ER70S-6 welding positions typical applications.
- [36] ER100S-G. Data sheet - bohler welding. 2014.
- [37] Ermakova A, Mehmanparast A, Ganguly S. A review of present status and challenges of using additive manufacturing technology for offshore wind applications. *Procedia Struct Integr* 2019;17:29–36.
- [38] Ermakova A, Mehmanparast A, Ganguly S, Razavi J, Berto F. Investigation of mechanical and fracture properties of wire and arc additively manufactured low carbon steel components. *Theor Appl Fract Mech* 2020;109:102685.
- [39] ASTM E647–13. Standard test method for measurement of fatigue crack growth rates. *Am. Soc. Test. Mater.* 2014:1–50. <https://doi.org/10.1520/E0647-15E01.2>.
- [40] American Society for Testing and Materials. ASTM E-1820-11: standard test method for measurement of fracture toughness. *Annu Book ASTM Stand* 2011:1–55. <https://doi.org/10.1520/E1820-18>.
- [41] Pi D, Ermakova A, Mehmanparast A. Numerical analysis of surface rolling effects on fatigue life enhancement of Wire Arc additively manufactured parts. *J Multiscale Model (JMM)* 2022:2146001. 1–16.
- [42] Pirling T, Bruno G, Withers PJ. SALSA—a new instrument for strain imaging in engineering materials and components. *Mater Sci Eng, A* 2006;437:139–44.
- [43] Jacob A, Oliveira J, Mehmanparast A, Hosseinzadeh F, Kelleher J, Berto F. Residual stress measurements in offshore wind monopile weldments using neutron diffraction technique and contour method. *Theor Appl Fract Mech* 2018;96:418–27.
- [44] Pynn R, Liang L. Neutron scattering—a non-destructive microscope for seeing inside matter. 2009. p. 15–36. [https://doi.org/10.1007/978-0-387-09416-8\\_2](https://doi.org/10.1007/978-0-387-09416-8_2).
- [45] Hutchings MT, Withers PJ, Holden TM, Lorentzen T. Introduction to the characterization of residual stress by neutron diffraction. *Introd. To charact. Residual Stress by Neutron Diffr* 2005. <https://doi.org/10.1201/9780203402818>.
- [46] Residual stress measurement by X-ray diffraction. 2003. Available at: <https://www.sae.org/publications/books/content/hs-784/2003/>. [Accessed 8 April 2022].
- [47] BSEN 15305. Non-destructive testing. Test method for residual stress analysis by X-ray diffraction - European Standards. 2008. Available at: <https://www.en-standard.eu/bs-en-15305-2008-non-destructive-testing-test-method-for-residual-stress-analysis-by-x-ray-diffraction/>. [Accessed 8 April 2022].
- [48] Mehmanparast A, Brennan F, Tavares I. Fatigue crack growth rates for offshore wind monopile weldments in air and seawater: SLIC inter-laboratory test results. *Mater Des* 2017;114:494–504.



- [49] Ermakova A, Mehmanparast A, Ganguly S, Razavi J, Berto F. Fatigue crack growth behaviour of wire and arc additively manufactured ER70S-6 low carbon steel components. *Int J Fract* 2021. <https://doi.org/10.1007/s10704-021-00545-8>.
- [50] Ermakova A, Ganguly S, Razavi J, Berto F, Mehmanparast A. Experimental investigation of the fatigue crack growth behavior in wire arc additively manufactured ER100S-1 steel specimens. *Fatig Fract Eng Mater Struct* 2021. <https://doi.org/10.1111/FFE.13598>.
- [51] Woo W, Kim DK, Kingston EJ, Luzin V, Salvemini F, Hill MR. Effect of interlayers and scanning strategies on through-thickness residual stress distributions in additive manufactured ferritic-austenitic steel structure. *Mater Sci Eng, A* 2019;744:618–29.
- [52] Woo W, An GB, Em VT, De Wald AT, Hill MR. Through-thickness distributions of residual stresses in an 80 mm thick weld using neutron diffraction and contour method. *J Mater Sci* 2014;50:784–93.
- [53] Gornyakov V, Ding J, Sun Y, Williams S. Understanding and designing post-build rolling for mitigation of residual stress and distortion in wire arc additively manufactured components. *Mater Des* 2022;213:110335.
- [54] Ganesh P, Sundar R, Kumar H, Kaul R, Ranganathan K, Hedao P, et al. Studies on fatigue life enhancement of pre-fatigued spring steel specimens using laser shock peening. *Mater Des* 2014;54:734–41.
- [55] Lu JZ, Luo KY, Zhang YK, Sun GF, Gu YY, Zhou JZ, et al. Grain refinement mechanism of multiple laser shock processing impacts on ANSI 304 stainless steel. *Acta Mater* 2010;58:5354–62.
- [56] Ryde L. Application of EBSD to analysis of microstructures in commercial steels. *Mater Sci Technol* 2006;22:1297–306.